



1 **Multi-mission altimetry data to evaluate hydrodynamic model-based stage-discharge**
2 **rating curves in flood-prone Mahanadi River, India**

3 Pankaj R. Dhote^{1,2,*}, Joshal K. Bansal¹, Vaibhav Garg¹, Praveen K. Thakur¹, Ankit Agarwal^{2,3,*}

4 ¹ Water Resources Department, Indian Institute of Remote Sensing, ISRO, Dehradun, India

5 ²Department of Hydrology, Indian Institute of Technology, Roorkee, India

6 ³GFZ German Research Centre for Geosciences, Helmholtz Centre, Potsdam, Germany

7

8 ***Correspondence:** Pankaj R. Dhote (pankaj_d@hy.iitr.ac.in), Ankit Agarwal
9 (ankit.agarwal@hy.iitr.ac.in)

10

11 **Highlights:**

- 12 • Multi-mission altimetry data used to validate rating curves
13 • Rating curves estimated using 1D-2D coupled hydrodynamic model
14 • Results confirmed marginal variation in performance of different altimeters
15 • Temporal resolution of altimeters does not affect reliability of water level

16

17

18

19

20

21

22



23

24 **Abstract**

25 River discharge and water level data play a vital role for various hydrological applications
26 worldwide. However, limited availability of in-situ data has drawn attention towards using
27 remote sensing techniques to monitor river flow. Indeed, multi-mission satellite altimetry
28 data has been used to generate stage-discharge rating curves through power-law relations
29 and empirical methods. The validation of hydrodynamic model-based rating curves is
30 missing. We investigate the potential of available altimetry series (Jason 2, Jason 3,
31 Saral/AltiKa, Sentinel 3A and Sentinel 3B) over Mahanadi River to validate the estimated
32 rating curves at virtual stations. The hydrodynamic model (HEC-RAS) was developed and 07
33 virtual stations were identified for Mahanadi River from Boudh to Mundali Barrage. During
34 calibration (July-October, 2018) and validation (July-October, 2018), Root Mean Square
35 Error (RMSE) and Nash-Sutcliffe Efficiency (NSE) between simulated and in-situ water level
36 was found to be (0.46 m, 0.83) and (0.45 m, 0.76) respectively. The calibrated and validated
37 model was used to generate rating curves at virtual stations. The RMSE ranging between 27
38 cm to 88 cm was observed between simulated and altimetry water levels, specifying the
39 potential of all the altimeters with varying specifications to validate the rating curves. The
40 rating curves estimated at virtual stations provide a cost-effective tool for monitoring river
41 flows at additional locations, producing discharge time series for various hydrological
42 applications and assessing of contribution of lateral tributaries.

43 **Keywords:** Satellite altimetry; Hydrodynamic modelling; Remote sensing; Mahanadi River;
44 Stage-discharge rating curves



45 **1. Introduction**

46 Monitoring and assessment of water resources within the watershed play a crucial role in
47 meeting human requirements and influencing socio-economic practices in industrial and
48 agricultural activities. The changing climate and resulting extreme hydrometeorological
49 events in recent decades have increased the frequency of natural disasters (e.g., flood,
50 drought) and stress on water resources (Alfieri et al., 2013; Banholzer et al., 2014; Oki &
51 Kanae, 2006). The hydrological and hydrodynamic models used for various applications (e.g.
52 hydrological forecasting, impact of climate change on water resources, flood risk
53 assessment) typically depends on water level and discharge to test the reliability of the
54 simulated outputs. Perhaps, field measurements over the many parts of the world are either
55 unavailable or sparsely available and decreasing due to the highly economical and temporal
56 efforts required for their maintenance (Andreadis et al., 2007; Bogning et al., 2018). The
57 data-scarcity issue becomes worsen in delta region of the rivers (e.g. Mahanadi River) and
58 high-mountain regions such as Himalayan river basins (Upper Ganga, Brahmaputra, Beas),
59 which experience recurrent flood hazard (Dhote et al., 2021; Kebede et al., 2020).

60 Spaceborne radar altimetry data has potentially monitored inland water bodies for more
61 than 25 years (Abdalla et al., 2021; Birkett et al., 2002). There are nadir looking altimeter
62 observations from the past (ENVISAT, Jason 1/2, Topex/Poseidon), present (Jason 3,
63 Saral/AltiKa - drifting phase since July 2016, Sentinel 3)(Calmant & Seyler, 2006; Paris et al.,
64 2016) and the forthcoming Surface Water and Ocean Topography (SWOT) missions (Durand
65 et al., 2010). Despite the challenges of inland water due to its complex surrounding
66 environment, long term altimetry data have been used to assess change in water level of



67 large rivers, lakes, wetlands and reservoirs (Dubey et al., 2015; Frappart et al., 2006; Thakur
 68 et al., 2021). The upcoming SWOT mission will collect data differently from previous
 69 missions. It consists of two wide swath radar interferometers KaRINs (Ka-band Radar
 70 INterferometers) separated by the nadir altimeter at the middle (Biancamaria et al., 2016;
 71 Durand et al., 2010; Fu et al., 2009). The SWOT will map waterbodies on a global scale, aiming
 72 to simultaneously provide high-resolution WSE, slope and river width for rivers wider than
 73 50-100 m. The repeat cycle of the SWOT will be of 21 days, allowing 2-4 visits at specific sites
 74 at regular intervals, dependent on the latitude.

75 Several previous studies revealed that radar altimetry could evaluate water levels in
 76 continental environments (Getirana & Peters-Lidard, 2013). The challenge is how to use this
 77 altimetry-based water level to estimate river discharge in addition to other methods based
 78 on remote sensing. The different approaches can be broadly classified as listed in Table 1.

79 **Table 1:** Methods to estimate river discharge using satellite altimetry

Approach	Remote Sensing Data	In-situ Data	References
generation of pseudo rating curves by application of power regression law using altimetry-based water level and in-situ discharge data	water level – altimetry observations	discharge (nearest station)	(Belloni et al., 2021; Dubey et al., 2015; Michailovsky et al., 2013; Papa et al., 2012; Rai et al., 2021; Zakharova et al., 2020)
use of modelled discharge and altimetry-based water to generate rating curves at virtual stations	water level – altimetry observations	discharge river cross-sections (bathymetry) roughness coefficients	(Leon et al., 2006; Paris et al., 2016; Tarpanelli et al., 2013)



calibration and validation of hydrodynamic models using satellite altimetry-based water levels	water level – altimetry observations	water level/ discharge river cross-sections (bathymetry) roughness coefficients	(Domeneghetti et al., 2021 ; Brêda et al., 2019; Chembolu et al., 2019; Domeneghetti et al., 2014; Getirana & Peters-Lidard, 2013; Milzow et al., 2011; Pereira-Cardenal et al., 2011; Wilson et al., 2007)
assimilation of altimetry-based water level to improve prediction potential of large-scale hydrological models	water level – altimetry observations	water level/ discharge river cross-sections (bathymetry) roughness coefficients	(Michailovsky et al., 2013; Paiva et al., 2013; Tourian et al., 2017)
the use of flow laws / empirical equations (Manning’s equation)	width – (optical/SAR/altimeters) water level – altimetry observations slope - altimetry observations	water level/ discharge river cross-sections roughness coefficients	(Garkoti and Kundapura, 2021 ; Tarpanelli et a., 2013; Zakharova et al.,2019Andreadis et al., 2007; Durand et al., 2016)

80

81 Based on the approaches listed in Table 1, researchers have exploited the satellite altimetry
 82 data using various approaches to estimate river discharge, generate rating curves and
 83 improve the prediction potential of hydrological-hydrodynamic models. Few approaches
 84 entirely depend on the in-situ data, while others exploit the altimetry observations with
 85 limited in-situ data. Water monitoring agencies often use developed stage-discharge rating
 86 curves (e.g. Central Water Commission, India) to estimate discharge corresponding to gauge-
 87 based water level. The rating curves developed by classical power regression law using in-
 88 situ stage-discharge data are limited to the gauging locations (Herschy, 1993). Further, the
 89 rating curves estimated using the hydrodynamic model provides various benefits over
 90 traditional approaches, such as considering water surface gradient, roughness coefficient
 91 changes, hydraulic factors etc. (Di Baldassarre and Montanari, 2009; Lang et al., 2010;
 92 Mansanarez et al., 2019). In this direction, Dhote et al., 2021 used a hydrodynamic model to
 93 estimate rating curves at virtual stations and validated those using single mission



94 Saral/AltiKa data. It is important to know that they used limited available daily in-situ data
95 to calibrate the hydrodynamic model and not altimetry data. Later, relatively coarse
96 temporal resolution (35 days) altimetry-based water levels were used to evaluate the
97 reliability of the rating curves at virtual stations. However, multi-mission satellite altimetry
98 data is yet to be tested to validate the hydrodynamic model-based rating curves.

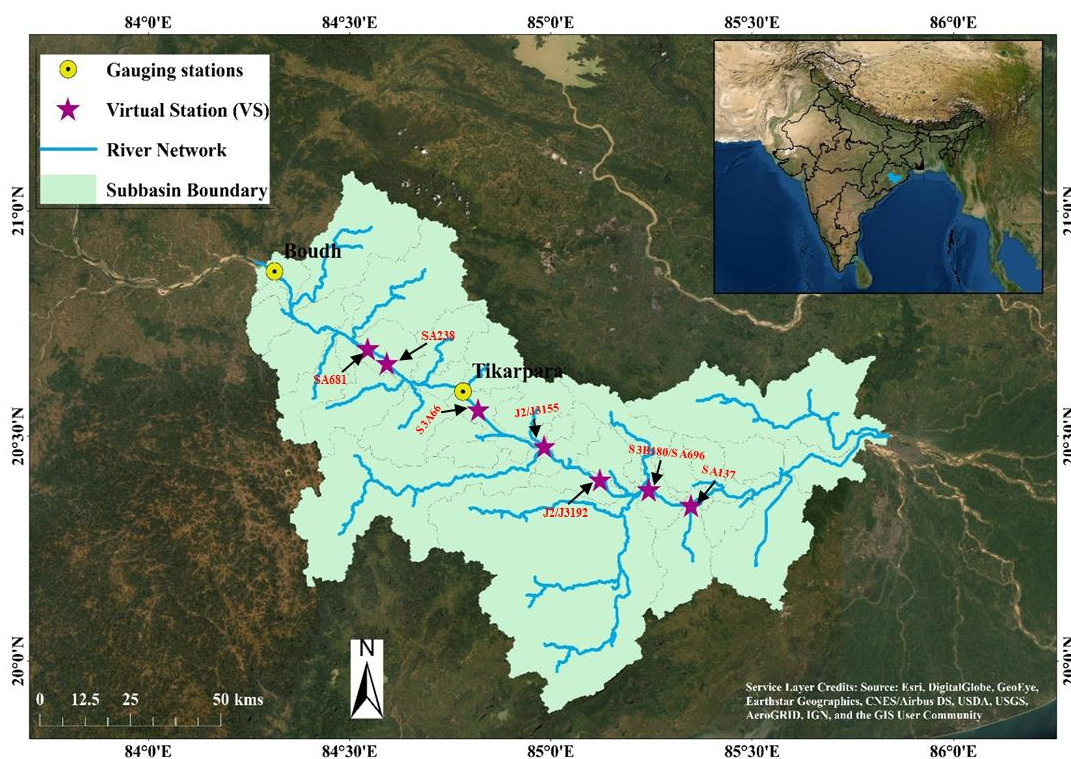
99 The present work proposes to estimate stage-discharge rating curves using a hydrodynamic
100 model and multi-mission satellite altimetry data (category c of Table 1). The analysis was
101 implemented on the Mahanadi River stretch from Boudh to Mundali Barrage (near Naraj),
102 where 7 virtual stations (10 passes) were identified. We specifically refer to altimeter data
103 from Jason 2 (J2), Jason 3(J3), Saral/AltiKa (SA), Sentinel 3A (S3A) and Sentinel 3B (S3B)
104 missions, which were used to retrieve water levels. The hydrodynamic simulations were
105 performed with HEC-RAS software package in a 1D-2D coupled configuration.

106 **2. Study area and data**

107 We focus on the 189 km river reach falling in the lower sub-basin of Mahanadi River, the
108 major inter-state river of India flowing east direction (Fig. 1). The Mahanadi is the 8th largest
109 basin having a total catchment area of 1.4×10^5 sq. km, covering 4.28% of the total
110 geographic area of India (CWC & NRSC, 2014). It covers a path of 851 km from an origin in
111 Dhamtari district of Chhattisgarh state until it drains into Bay of Bengal. The analysis in this
112 study focuses on the river reach bounded by gauging station Boudh at upstream and Mundali
113 barrage (near Naraj) at downstream end. Right after the Mundali, delta region of the
114 Mahanadi River starts which experiences severe floods frequently in monsoon season
115 (Samantaray and Sahoo, 2020; Jena et al., 2014). The extreme rainfall events induced flood



116 waves and low main channel carrying capacity at the upstream region, leading to recurrent
117 flood havoc in the delta region. As per Parhi et al., 2012, 69 % of major floods events (1960-
118 2011) in the delta region are due to uncontrolled streamflow from the catchment area above
119 delta head Mundali. Further, relatively low-lying area aggregates the flood situation in this
120 region.



121

122 **Fig.1.** Mahanadi River stretch (Boudh to Mundal Barrage) considered in the study along with
123 locations of gauging stations, outlet and identified virtual stations (VSs) from multi-mission
124 altimetry data (Background image credits: Esri, DigitalGlobe, GeoEye, Earthstar Geographics,
125 CNES/Airbus DS, USDA, USGS, AEX, Getmapping, Aerogrid, IGN, IGP, swisstopo, and the GIS
126 User Community)

127

128 The different satellite altimetry missions data considered in this study are Jason 2, Jason 3,
129 Saral/AltiKa, Sentinel 3A and Sentinel 3B (Table 2). The locations of virtual stations (07), VSs



130 (locations where altimeter tracks cross the river) considered in this study are shown in Fig.1.
131 Radiometrically Terrain Corrected (RTC) ALOS PALSAR DEM with a spatial resolution of 12.5
132 m was downloaded from Alaska Satellite Facility. This RTC DEM (released in 2014) is
133 generated from ALOS PALSAR L1.1 image and global SRTM DEM (GL1: 30 m resolution)
134 having accuracy as 20 m CE90 (Horizontal circular error at 90th percentile); 16 m LE90
135 (Vertical linear error at 90th percentile). Land use land cover (LULC) map prepared under
136 the Indian Space Research Organization-International Geosphere Biosphere (ISRO-IGBP)
137 Programme was procured from the National Remote Sensing Centre (NRSC), ISRO,
138 Hyderabad, India. (NRSC, 2006).

139 The stage-discharge data required for hydrodynamic model setup was obtained from Central
140 Water Commission (CWC), Bhubaneswar, Odisha State, India. The gauge data of three
141 stations, namely, Boudh, Tikarpara and Naraj and discharge data of Boudh and Tikarpara
142 stations were obtained. The surveyed river cross-sections (12) of Mahanadi River from
143 Boudh to Naraj were procured from CWC, Bhubaneswar.

144 **Table 2:** Satellite altimetry data used in the study

Mission	Temporal Resolution (day)	Height (m)	Inclination (degrees)	Source
Jason 2	9.91	1336	66	AVISO
Jason 3	10	1336	66	AVISO
Saral/AltiKa	35	800	98.5	AVISO
Sentinel 3A	27	814.5	95.65	COPERNICUS
Sentinel 3B	27	814.5	95.65	COPERNICUS

145

146



147 **3. Methods**

148 The entire methodology used in this study is divided into two parts. The first part involves
149 preparing different input layers to set up a hydrodynamic model using geospatial data and
150 field observations. The stage-discharge rating curves were generated at virtual stations
151 using a hydrodynamic model. The second part includes retrieving water levels from the
152 multi-mission satellite altimeters like SARAL/AltiKa, Jason-2/3, Sentinel-3A/3B using
153 Python & BRAT. The estimated water levels were used to evaluate the hydrodynamic-model
154 based rating curves.

155 **3.1 Model setup**

156 Extensively used freely available physically based hydrodynamic model HEC-RAS (Bruner,
157 2016) was used to carry out numerical simulations of river reach in 1D-2D coupled
158 configuration. HEC-RAS software provides a solution to full 1D Saint-Venant equations using
159 four-point implicit finite difference technique. In contrast, full 2D Saint-Venant equations are
160 solved using an implicit finite volume algorithm (Bruner, 2016). The 1D-2D coupled
161 configuration used in this study enabled an option to simulate 2D flow dominating region
162 near delta (downstream end, Mundali barrage) using 2D mode and approximate relatively
163 unidirectional flow in rest river reach using 1D mode. This model setup arrangement
164 facilitated the exploitation of both schemes' advantages, reducing computational time.
165 Various studies have been carried out to evaluate the suitability of 1D, 2D, and 1D-2D
166 coupled hydrodynamic models (Ghimire et al., 2022; Shustikova et al., 2019; Dhote et al.,
167 2019); however, detailed analysis on topographic input data, processes and output
168 uncertainties is not within the scope of this study.



169 The different steps followed to set up the model are discussed below:

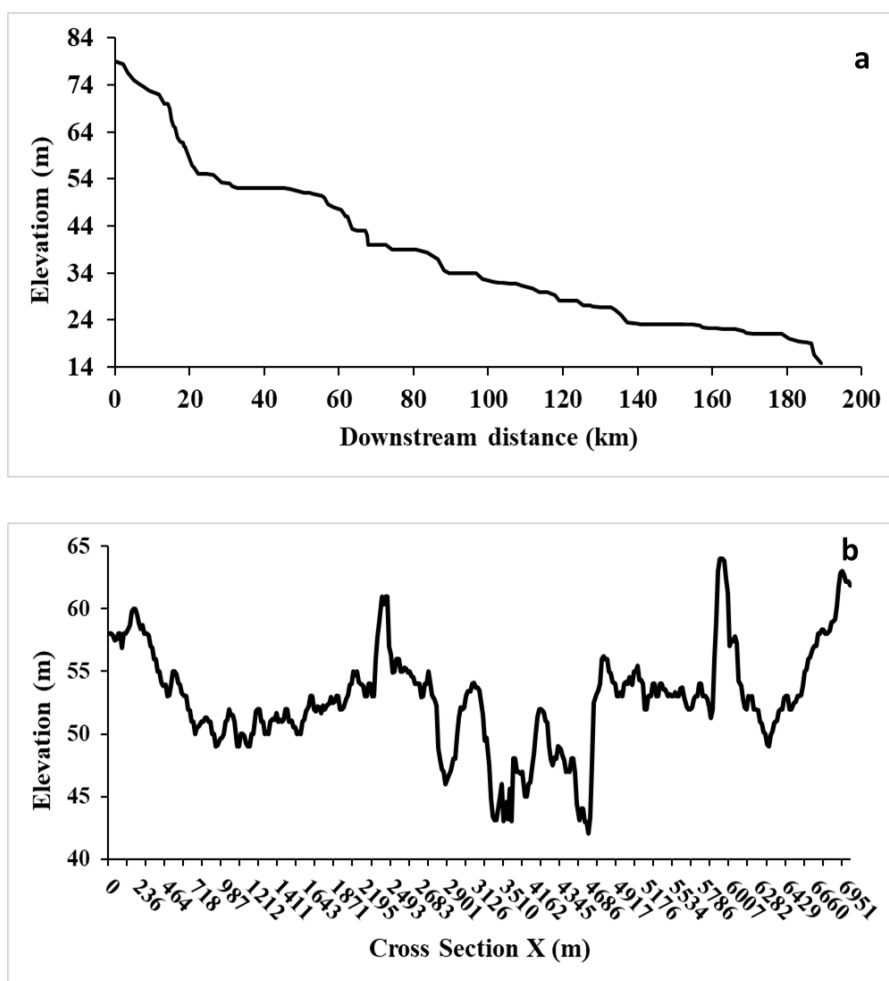
170 1) **River network profile:** River network was digitized from Boudh to Mundali barrage
171 using high-resolution images of Google Earth in the RAS Mapper module of HEC-RAS.
172 Later, a digitized river file can also be imported in various formats (.shp, .kml) in other
173 GIS platforms.

174 2) **Channel-floodplain geometry:** To set up the 1D model, river cross-sections and
175 elevation profiles (left to right bank) were extracted from ALOS PALSAR DEM using
176 the tool available in HEC-RAS. The length of cross-sections was varied to ensure the
177 coverage of floodplain and main channel geometry. Initially, cross-sections were
178 extracted at 500 m spacing in automated mode from Boudh to Mundali barrage. Later
179 few cross-sections were added/deleted/edited to account for the meandering of the
180 river. To represent geometry of 2D flow dominating area near delta-head Mundali, 2D
181 floodplain mesh was generated using ALOS-PALSAR DEM. We specifically
182 represented the floodplain of flood-prone tributaries Kusumi and Rana (kindly refer
183 to Fig. 3 and Boundary condition section) as 2D domain. The lateral structure was
184 used to connect 2D flow areas with 1D main river.

185 The topography of the floodplain can be well displayed with spaceborne DEM, but
186 bathymetry is rather difficult to represent. Thus, we used the closest surveyed river
187 cross-section data to modify the DEM-based cross-sections. Only 12 surveyed cross-
188 sections were available at an uneven spacing from Boudh to Mundali, first used to
189 correct DEM-based cross-sections. As surveyed cross-sections are referenced to local
190 datum, mean sea level (msl), datum correction was applied ranging from - 0.06 m to
191 +6.2 m. Later, modified bathymetry was interpolated among other intermediate



192 cross-sections. This resulted in hybrid cross-sections (Dhote et al., 2021) used to
193 model setup. The longitudinal profile of the main river channel and typical hybrid
194 cross-section at 102 km chainage is shown in Fig 2.

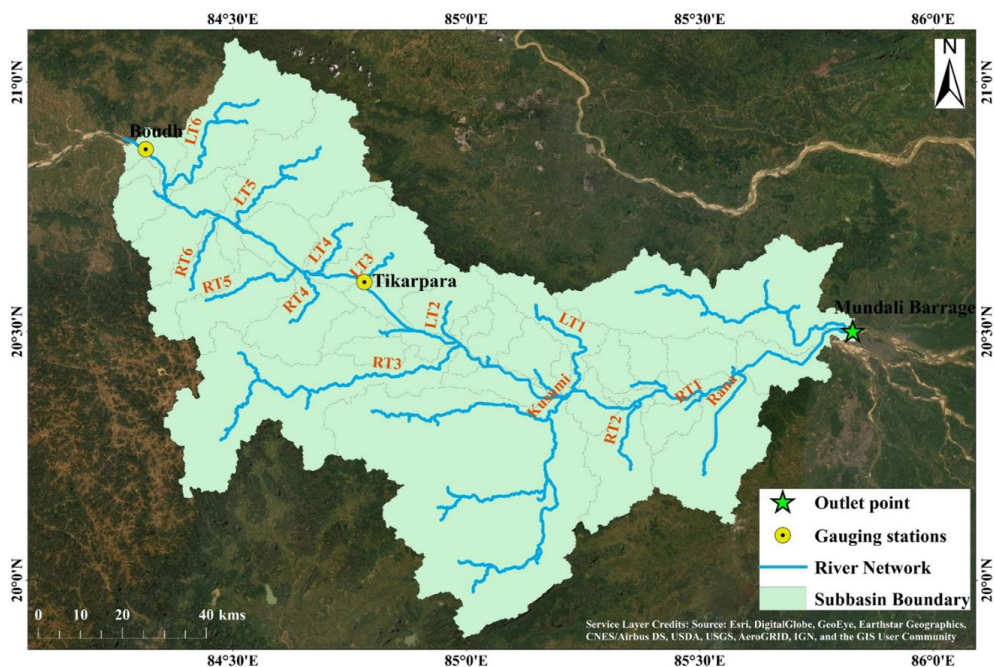


195
196 **Fig.2.** (a) Main channel longitudinal profile from Boudh to Mundali Barrage (b) Hybrid cross-
197 section at 102 km chainage from Boudh station

198
199
200



201 **3. Boundary conditions:** In this study, discharge hydrograph was provided as a
202 boundary condition at all upstream nodes of the river network, while normal depth
203 was provided at the downstream end (Mundali). However, in-situ discharge data
204 were available at limited locations within the study area (Fig.1). Considering the
205 importance of upstream boundary conditions on the accuracy of the model, the
206 contribution of lateral tributaries (Fig. 3) was estimated using the discharge-area
207 ratio method. In this method, discharge data for each tributary was estimated by
208 multiplying drainage- area ratio (= watershed area of tributary/watershed area
209 concerning Tikarpara) with discharge data at Tikarpara. The contribution of each
210 tributary is shown in Table 3, highlighting that the contribution of right bank
211 tributaries near the delta region, namely Kusumi and Rana, is on the relatively higher
212 side.



213



214 **Fig. 3.** Mahanadi river tributaries contributing between Boudh and Mundali Barrage
215 (Background image credits: Esri, DigitalGlobe, GeoEye, Earthstar Geographics,
216 CNES/Airbus DS, USDA, USGS, AEX, Getmapping, Aerogrid, IGN, IGP, swisstopo, and
217 the GIS User Community)

218

219 **Table 3.** Contribution of the tributaries

Tributary	Catchment Area (Sq. km)	Contribution in % using drainage-area ratio method
Rana	499	4.96
RT1	103	1.18
RT2	289	2.87
Kusumi	2117	21.07
RT3	1009	10.04
RT4	269	2.68
RT5	287	2.86
RT6	205	2.04
LT1	225	2.23
LT2	205	2.03
LT3	213	2.11
LT4	195	1.94
LT5	540	5.37
LT6	528	5.25

220

221 **4. Roughness coefficients:** The lookup table was created to relate the surface
222 roughness coefficient (Manning's n , $m^{-1/3} s$) with varying land use land cover. The
223 ISRO IGBP LULC and high-resolution images of Google Earth were used to identify
224 different classes within a floodplain. The literature and previously published work
225 was used to select n values (Chow et al., 1998; Parhi et al., 2013). The n value varied
226 from 0.05 to 0.2 $m^{-1/3} s$ for various classes in the floodplain, while the initial n for the
227 main channel was kept as 0.035 $m^{-1/3} s$.

228 **5. Simulations:** Hydrodynamic model was set up for a river stretch of 189 km from



229 Boudh to Mundali barrage, constrained with discharge data as a boundary condition
230 at upstream nodes and normal depth at the downstream end. We ran this developed
231 model in two phases: calibration and validation corresponding to extreme flood
232 events within available data. The model was calibrated using daily observation for
233 the 2015 monsoon season (July-October). During the calibration phase, a model was
234 simulated for multiple sets by spatially varying the main river channel Manning's n in
235 successive iterations (Dhote et al., 2019; Domeneghetti et al., 2021) and calculated
236 the goodness-of-fit. The Root Mean Square Error (RMSE) and Nash-Sutcliffe Efficiency
237 (NSE) were used as the goodness-of-fit criteria between simulated and observed
238 water levels at Tikarpara station. The optimized value of Manning's n of the channel
239 (keeping n constant for floodplain classes) producing the lowest RMSE and highest
240 NSE was identified during calibration. The model was validated by performing the
241 boundary conditions for a period not included in the calibration phase (July to
242 October 2018), and subsequently estimated statistical parameters. Later, the stage-
243 discharge rating curve was estimated at each virtual station corresponding 2018
244 flood event.

245

246 ***3.2 Retrieval of water level using satellite altimetry data***

247 Radar altimetry is an advanced remote sensing technique to estimate the water level of
248 inland water bodies. In this study, virtual stations were identified based on tracks of multi-
249 mission altimetry data (Jason 2, Jason 3, SARAL/AltiKa, Sentinel 3A and Sentinel 3B) falling
250 between Boudh and Mundali along Mahanadi River. It was found that 8 virtual stations can
251 be established using data from 10 altimetry tracks having varying time duration (same



252 virtual station /pass for Jason 2 and Jason 3 tracks, see Table 4). To retrieve water level using
253 altimetry data, first of all, we need satellite orbit altitude (Alt) and the altimeter range value
254 (R). A retracing algorithm is applied to correct the range value (R), as the leading edge of the
255 waveform diverges from the defined onboard altimeter gate. We used a standard Off-Center
256 of gravity (OCOG) retracking algorithm to correct the range. Various geophysical corrections
257 (dry tropospheric correction, wet tropospheric correction, ionospheric correction) to
258 account for time delay of microwave pulses due to atmospheric effects, correction for pole
259 and solid tidal effects on the Earth were applied to correct retrieved water level (Chelton et
260 al., 2001; Wahr,1985; Cartwright and Edden,1973). The equation relating different terms to
261 estimate water level is given below. We calculated the orthometric height considering EGM
262 96 as datum because different altimetry missions use different reference ellipsoids.

$$263 \quad H = Alt - R - (D_{tc} + W_{tc} + I_{onc} + S_{tc} + P_{tc}) - MSS_{ht} \quad (1)$$

264 Where H: corrected orthometric height; Alt: the satellite altitude from reference ellipsoid; R:
265 the satellite range; D_{tc} : the dry tropospheric correction; W_{tc} : the wet tropospheric
266 correction; I_{onc} : the ionospheric correction; S_{tc} : the solid tide; P_{tc} : the pole tide correction;
267 and MSS_{ht} : the mean sea surface from the reference ellipsoid.

268 **Table 4:** Virtual stations identified based on the altimeter passes

Sl. No.	Satellite	Pass	Data Availability	Nearest Location
1	Jason 2	155	2008-2015	Kanasinga
2	Jason 2	192	2008-2015	Mahukana
3	Jason 3	155	2016-Present	Kanasinga
4	Jason 3	192	2016-Present	Mahukana
5	Sentinel 3A	66	2016-Present	Mahakudpalli
6	Sentinel 3B	180	2018-Present	Khaparmala



7	SARAL/AltiKa	137	2013-2016	Badabar
8	SARAL/AltiKa	238	2013-2016	Dubapalli
9	SARAL/AltiKa	681	2013-2016	Badhupalli
10	SARAL/AltiKa	696	2013-2016	Khaparmala

269

270 **4. Results and discussion**

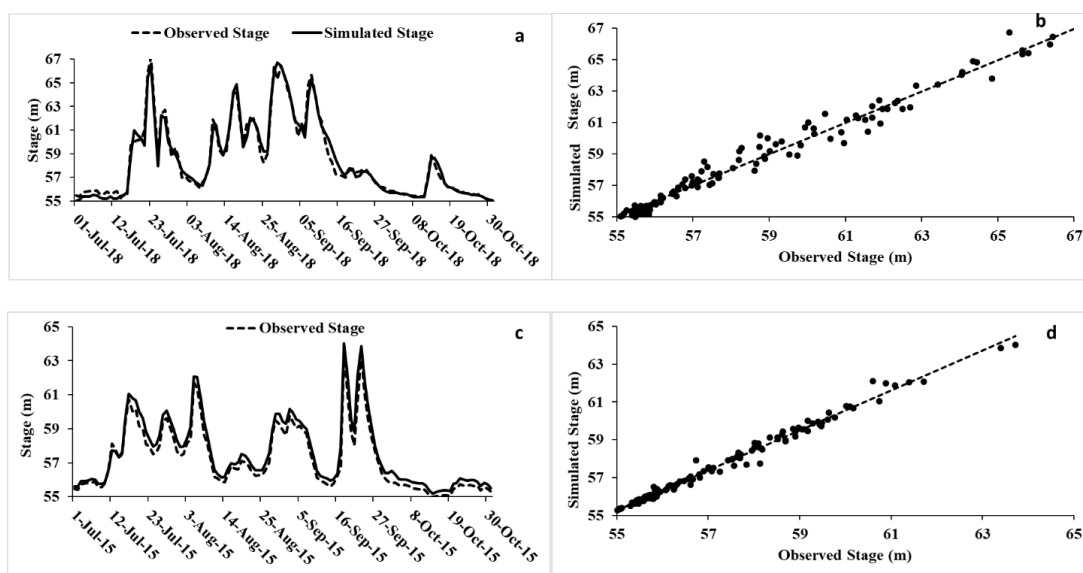
271 Here we present the findings of calibration and validation of hydrodynamic model (a); and
272 the use of available altimetry series to validate the model-based stage-discharge rating
273 curves (b).

274 ***4.1 Calibration and validation of the model***

275 The calibration and validation of the model were carried out for extreme monsoon events,
276 respectively, for 2018 and 2015, at a daily time scale. The channel n value was varied from
277 0.02 to 0.06 $\text{m}^{-1/3} \text{s}$, until there was good agreement between simulated and observed water
278 levels at Tikarpara station (Chow et al., 1988; Horritt and Bates, 2002; Dhote et al., 2019).
279 During calibration, the comparison of simulated and observed water levels at Tikarpara
280 produced minimal RMSE (0.46 m) and high NSE (0.83) corresponding to optimized n value
281 of 0.03 $\text{m}^{-1/3} \text{s}$ (Fig. 4). Parhi, 2013 evaluated the channels n value of the HEC-RAS model to
282 simulate extreme flood events peak discharge and time of peak in Mahanadi River basin.
283 They showed that, Manning's n of 0.029 lead to lowest error of 5.42%, thus validating our
284 calibration performance. It is worth mentioning that, observed water level is reference to
285 local datum (msl), while datum of simulated water level is EGM 96. Thus, datum correction
286 of -0.79 m was applied to the observed stage before comparative assessment. Fair agreement



287 during independent boundary condition of validation year 2015 (RMSE 0.45 m ; NSE 0.76),
288 suggested good performance of hydrodynamic model (Fig 4).



289

290 **Fig. 4.** Calibration (a, b, during year 2018) and validation (c, d, during year 2015) of the
291 hydrodynamic model at Tikarpara.

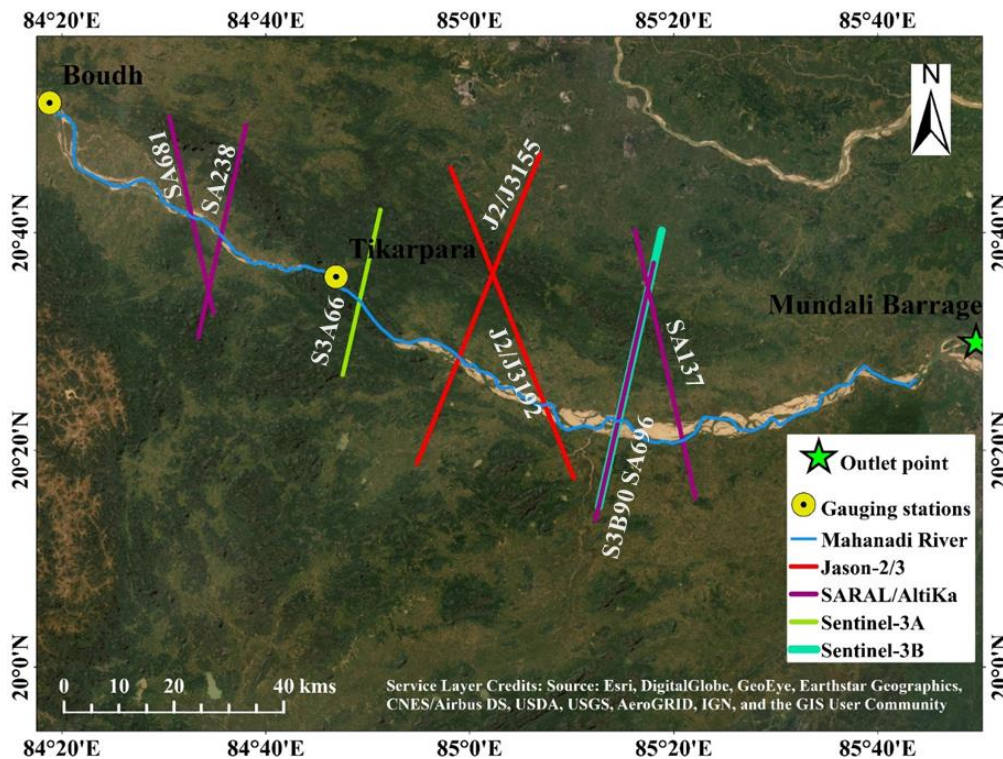
292

293 **4.2 Multi-mission satellite altimetry observations to evaluate model-based stage-** 294 **discharge rating curves**

295 Observations from multi-mission altimeter tracks provide an opportunity to study water
296 level dynamics (courser temporal resolution) at additional locations compared to in-situ
297 gauging stations. The challenging question is how efficiently river discharge can be
298 monitored at these locations (virtual stations, see Fig. 5). The rating curves were estimated
299 at 07 virtual stations using hydrodynamic simulations for extreme flood events during



300 monsoon seasons 2018 and 2015. The comparative assessment was carried out between
301 simulated and altimetry-based water levels at virtual stations.



302
303 **Fig.5.** Virtual stations identified using tracks of satellite altimeters over the river stretch
304 (Background image credits: Esri, DigitalGlobe, GeoEye, Earthstar Geographics, CNES/Airbus
305 DS, USDA, USGS, AEX, Getmapping, Aerogrid, IGN, IGP, swisstopo, and the GIS User
306 Community)

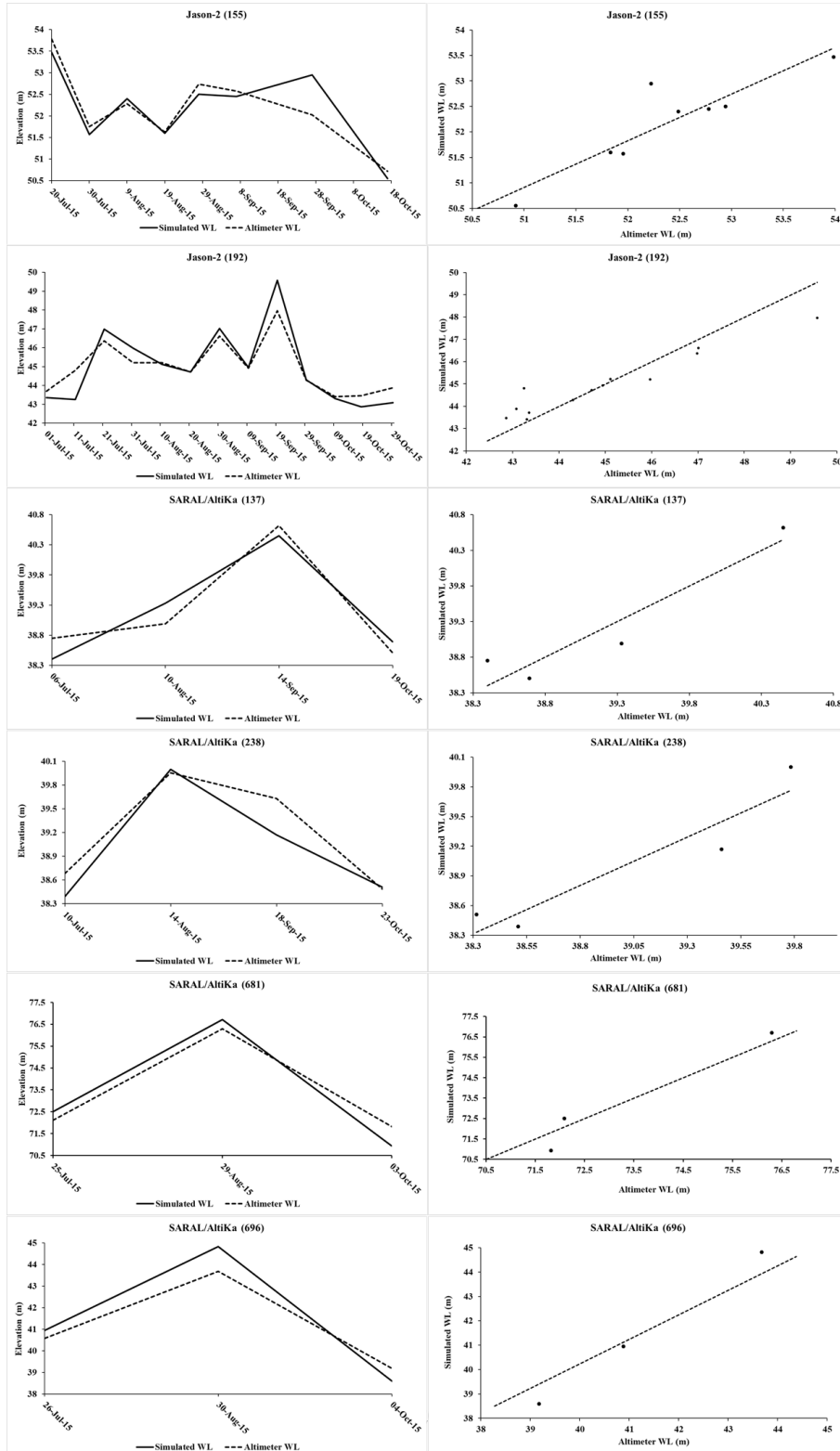
307 The simulated model was found to agree with altimeter-based water levels (after applying
308 bias correction) among all the altimetry datasets with different durations (Fig. 6, 7 and Table
309 5). In general, simulated water levels followed altimeter observations with high accuracy,
310 showing NSE always more significant than 0.76. Even though variation in errors during



311 comparison were very marginal, Saral/AltiKa showed the lowest error (average RMSE 0.49
 312 m), followed by Jason 02 (0.58 m), Sentinel 3 (0.72 m) and Jason 3 (0.74 m). Moreover, the
 313 temporal resolution of altimeters ranging from 10 days to 35 days did not affect the
 314 reliability of the estimated water levels. This compassion at virtual stations ensures the
 315 validation of estimated rating curves (Fig. 8). These rating curves can be utilized as a virtual
 316 gauging network (in addition to in-situ stations), facilitating a cost-effective tool for
 317 monitoring river flows at additional locations, producing discharge time series for various
 318 hydrological applications, and assessing the contribution of lateral tributaries.

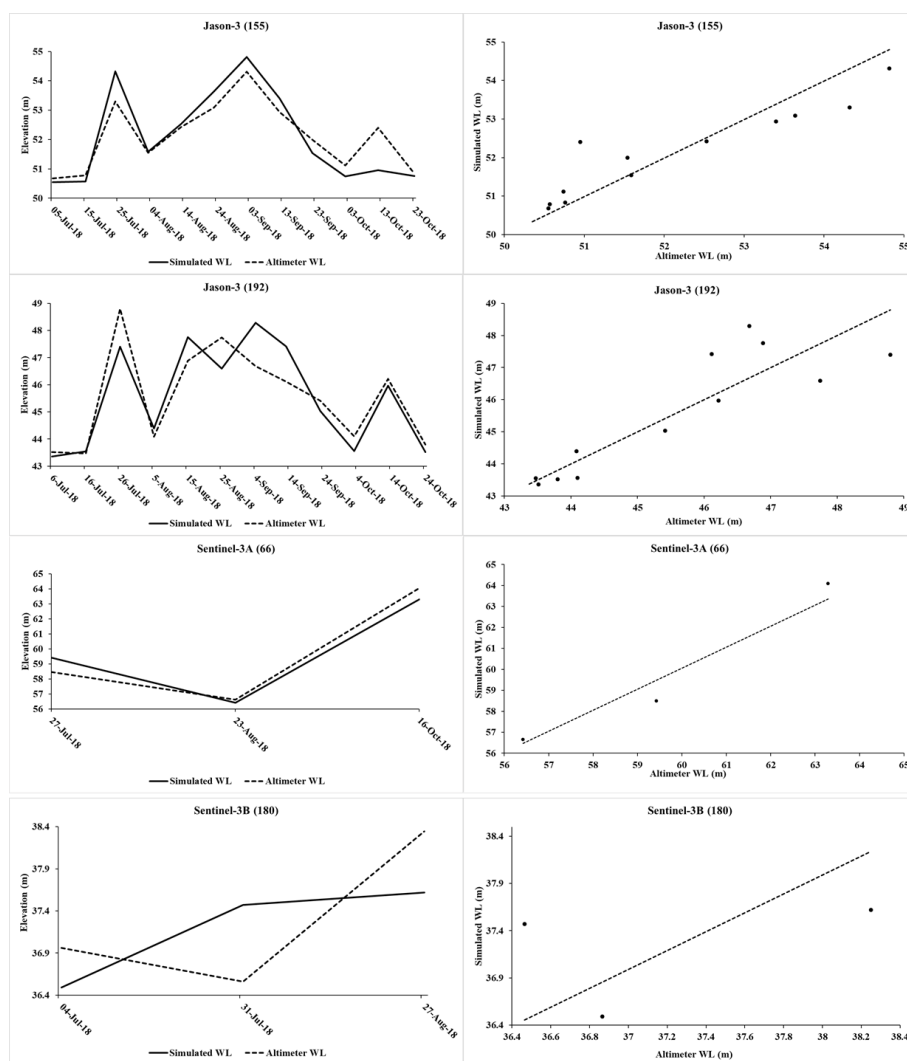
319 **Table 5:** Statistics of the comparison between satellite altimetry water level and modelled
 320 water level

Satellite	Pass	NSE	RMSE (m)	Bias Correction (m)
Jason 2	155	0.76	0.42	-0.204
Jason 2	192	0.84	0.74	-0.009
Jason 3	155	0.83	0.60	+0.035
Jason 3	192	0.76	0.88	-0.173
Sentinel 3A	33	0.93	0.72	-0.045
Sentinel 3B	90	0.94	0.72	-0.094
SARAL/AltiKa	137	0.76	0.35	+0.270
SARAL/AltiKa	238	0.81	0.27	-0.171
SARAL/AltiKa	681	0.93	0.60	-0.0225
SARAL/AltiKa	696	0.90	0.77	+0.307





322 **Fig.6.** Comparison of the simulated and altimetry-based water level during the year 2015 (black
 323 dotted lines in right panes indicates 1:1 line)
 324

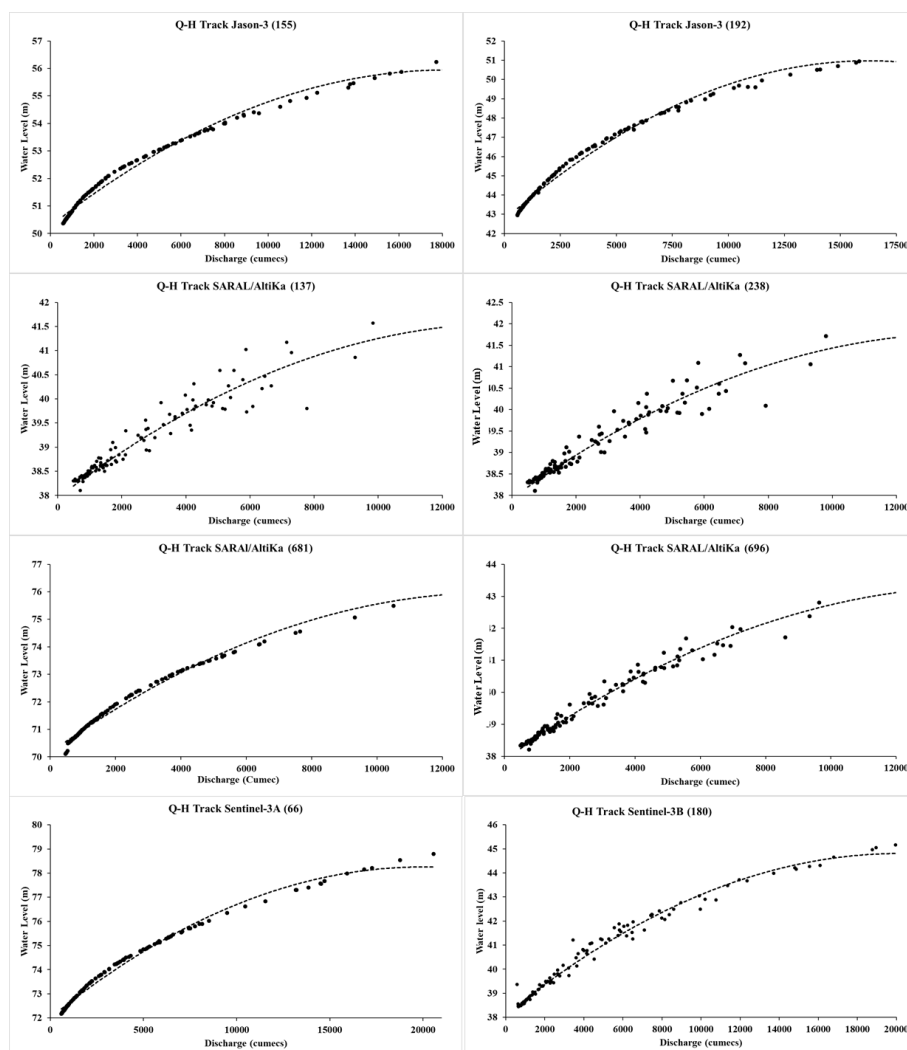


325

326 **Fig.7.** Comparison of the simulated and altimetry-based water level during the year 2018 (black
 327 dotted lines in right panes indicates 1:1 line).
 328



329 The altimetry-based water level has been the most exploited remote sensing data to estimate
330 river discharge. Most of these approaches (see Table 1) use altimeter data along with the
331 limited in-situ data to develop rating curves. The proposed framework in this study ensures
332 estimation of relatively accurate rating curves, however, restricts its application in ungauged
333 basins. Mere comparison of water levels at virtual stations does not rule out uncertainty
334 associated with the estimated discharge. However, as model was already calibrated and
335 simulated water levels mimicked satellite observations accurately, we can rely on estimated
336 discharge produced from modelled stage-discharge relation (Dhote et al., 2021). The outputs
337 of the physically-based models are governed by adopted modelling scheme and model
338 parameterization. Perhaps, rating curves based on these models (HEC-RAS) eliminates the
339 uncertainty associated with other empirical /power law approaches (Garkoti and
340 Kundapura, 2021 ; Tarpanelli et a., 2013) such as constant roughness coefficient, influence
341 of drainage area, overflows of the banks. Thus, it is tough to remove all the errors but we
342 must be aware of degree of uncertainty associated with the adopted approach. Further, as
343 the proposed framework is generic, it can implemented on the high-mountains data-scarce
344 Himalayan river basins. It will be interesting to evaluate the impact of hilly terrain on
345 accuracy of the altimetry-based water levels and its application to generate stage-discharge
346 rating curves. This could be the potential future work.



347

348 **Fig. 8.** Rating curves generated at virtual stations using the hydrodynamic model run during
349 the monsoon season of the year 2018 (07 rating curves corresponding 10 altimetry tracks:
350 Pass 155 shared by J2 and J3, Pass 190 shared by J2 and J3, S3B180 shared by SA696).

351
352
353
354
355
356
357
358
359



360 **5. Conclusions**

361 The present work investigated the use of multi-mission altimeter data to validate the model-
362 based stage-discharge rating curves in Mahanadi River, India. Using hydrodynamic
363 modelling simulations, the rating curves were estimated at 7 virtual stations falling between
364 Boudh and Mundali barrage. The altimeter data from different missions such as Jason 2,
365 Jason 3, Saral/AltiKa, Sentinel 3A and Sentinel 3B were used to retrieve water levels at these
366 virtual stations. The statistical indicators (RMSE 0.27-0.88 m, NSE 0.76-0.94) revealed that
367 simulated water levels could reproduce altimeter observations at these virtual stations with
368 high agreement. Even though the temporal resolution of altimeters ranged from 10 days to
369 35 days, no substantial implications on the reliability of the water level were observed. The
370 rating curves estimated at virtual stations can be utilized as a virtual gauging network (in
371 addition to in-situ stations), facilitating a cost-effective tool for monitoring of river flows at
372 additional locations, producing discharge time series for various hydrological applications
373 and assessment of the contribution of lateral tributaries.

374 **Acknowledgement**

375 The authors would like to thank Central Water Commission (CWC), India, for providing
376 topographic and hydrometric data. We are grateful to Alaska Satellite Facility (ASF), Aviso,
377 Copernicus portals, and Environmental Systems Research Institute (ESRI) for providing
378 topographic, altimeter, and high-resolution base maps, respectively. This work is partially
379 funded by the Indian Space Research Organization (ISRO), India, under Technology
380 Development Programme (TDP) project "Flood-prone Areas Identification and Flood Risk
381 Assessment using Integrated Process-based Modelling and Geospatial Techniques".



Authorship Contribution Statement:

Pankaj R. Dhote: Conceptualization, Funding acquisition, Investigation, Methodology, Data Analysis, Writing – original draft. **Joshal K. Bansal:** Conceptualization, Methodology, Data curation, Formal analysis, Visualization, Writing – original draft. **Vaibhav Garg:** Conceptualization, Methodology, Supervision, Writing – review & editing. **Praveen K. Thakur:** Conceptualization, Supervision, Writing – review & editing. **Ankit Agarwal:** Conceptualization, Supervision, Writing – review & editing.

382 Data availability:

383 Processed data may be shared on request by contacting contact authors.

384 Declaration of Competing Interest

385 The authors declare that they have no known competing financial interests or personal
386 relationships that could have influenced the work reported in this paper.

387

388 References:

- 389 Abdalla, S., Abdeh Kolahchi, A., Ablain, M., Adusumilli, S., Aich Bhowmick, S., Alou-Font, E., Amarouche, L.,
390 Andersen, O. B., Antich, H., Aouf, L., Arbic, B., Armitage, T., Arnault, S., Artana, C., Aulicino, G., Ayoub, N.,
391 Badulin, S., Baker, S., Banks, C., ... Zlotnicki, V. (2021). Altimetry for the future: Building on 25 years of
392 progress. *Advances in Space Research*, 68(2), 319–363. <https://doi.org/10.1016/j.asr.2021.01.022>
- 393 Alfieri, L., Burek, P., Dutra, E., Krzeminski, B., Muraro, D., Thielen, J., & Pappenberger, F. (2013). GloFAS-global
394 ensemble streamflow forecasting and flood early warning. *Hydrology and Earth System Sciences*, 17(3),
395 1161–1175. <https://doi.org/10.5194/HESS-17-1161-2013>
- 396 Andreadis, K. M., Clark, E. A., Lettenmaier, D. P., & Alsdorf, D. E. (2007). Prospects for river discharge and depth
397 estimation through assimilation of swath-altimetry into a raster-based hydrodynamics model. *Geophys Res*
398 *Lett*, 34(10), L10403. <https://doi.org/10.1029/2007gl029721>
- 399 Banholzer, S., Kossin, J., & Donner, S. (2014). The Impact of Climate Change on Natural Disasters. *Reducing*
400 *Disaster: Early Warning Systems for Climate Change*, 9789401785983, 21–49. [https://doi.org/10.1007/978-](https://doi.org/10.1007/978-94-017-8598-3_2)
401 [94-017-8598-3_2](https://doi.org/10.1007/978-94-017-8598-3_2)



- 402 Belloni, R., Camici, S., & Tarpanelli, A. (2021). Towards the continuous monitoring of the extreme events through
403 satellite radar altimetry observations. *Journal of Hydrology*, 603.
404 <https://doi.org/10.1016/j.jhydrol.2021.126870>
- 405 Biancamaria, S., Lettenmaier, D. P., & Pavelsky, T. M. (2016). The SWOT Mission and Its Capabilities for Land
406 Hydrology. *Surveys in Geophysics*, 37(2), 307–337. [https://doi.org/10.1007/S10712-015-9346-](https://doi.org/10.1007/S10712-015-9346-4)
407 [Y/FIGURES/6](https://doi.org/10.1007/S10712-015-9346-4)
- 408 Birkett, C. M., Mertes, L. A. K., Dunne, T., Costa, M. H., & Jasinski, M. J. (2002). Surface water dynamics in the Amazon
409 Basin: Application of satellite radar altimetry. *Journal of Geophysical Research: Atmospheres*, 107(20), LBA
410 26-1-LBA 26-21. <https://doi.org/10.1029/2001JD000609>
- 411 Bogning, S., Frappart, F., Blarel, F., Niño, F., Mahé, G., Bricquet, J. P., Seyler, F., Onguéné, R., Etamé, J., Paiz, M. C., &
412 Braun, J. J. (2018). Monitoring water levels and discharges using radar altimetry in an ungauged river basin:
413 The case of the Ogooué. *Remote Sensing*, 10(2). <https://doi.org/10.3390/rs10020350>
- 414 Brêda, J. P. L. F., Paiva, R. C. D., Bravo, J. M., Passaia, O. A., & Moreira, D. M. (2019). Assimilation of Satellite Altimetry
415 Data for Effective River Bathymetry. *Water Resources Research*, 55(9), 7441–7463.
416 <https://doi.org/10.1029/2018WR024010>
- 417 Brunner, G.W. (2016). "HEC-RAS, river analysis system hydraulic reference manual." Version 5.0, US Army Corps
418 of Engineers Hydrologic Engineering Center, Davis, CA, 547
- 419 Calmant, S., & Seyler, F. (2006). Continental surface waters from satellite altimetry. *Comptes Rendus Geoscience*,
420 338(14–15), 1113–1122. <https://doi.org/10.1016/j.crte.2006.05.012>
- 421 Cartwright, D. E., Edden, A.C., 1973. Corrected tables of tidal harmonics. *Geophysical Journal International*,
422 33(3):253–264.
- 423 Chelton, D.B., Ries, J.C., Haines, B.J., Fu, L.L., Callahan, P.S., 2001. Satellite altimetry. In: Fu, L.-L., Cazenave, A. (Eds.),
424 *Satellite Altimetry and Earth Sciences*. Academic, San Diego CA, pp. 1–131.
- 425 CWC & NRSC, 2014. Mahanadi River basin report prepared by Central Water Commission (CWC) and National
426 Remote Sensing Centre (NRSC), ISRO, New Delhi.
- 427 Chembolu, V., Dubey, A. K., Gupta, P. K., Dutta, S., & Singh, R. P. (2019). Application of satellite altimetry in
428 understanding river–wetland flow interactions of kosi river. *Journal of Earth System Science*, 128(4), 1–15.
429 <https://doi.org/10.1007/S12040-019-1099-4/TABLES/6>
- 430 Chow, V.T., Maidment, D.R., Mays, L.W., (1988). *Surface Water*. In: Applied Hydrology, 1st ed., McGraw-Hill
431 Science: Columbus, OH, USA, 127–166
- 432 Dhote P.R., Thakur P.K., Domeneghetti A., Chouksey A., Garg V., Aggarwal S.P., Chauhan P. (2021). The use of
433 SARAL/AltiKa altimeter measurements for multi-site hydrodynamic model validation and rating curves
434 estimation: An application to Brahmaputra River, *Advances in Space Research*, 68(2), 691-702.
435 <https://doi.org/10.1016/j.asr.2020.05.012>.
- 436 Dhote, P.R., Aggarwal, S.P., Thakur, P.K., Garg, V., 2019. Flood inundation prediction for extreme flood events: a
437 case study of Tirthan River, North West Himalaya. *Himalayan Geol.* 40 (2), 128–140.
- 438 Di Baldassare, G., Montanari, A., 2009. Uncertainty in river discharge observations: a quantitative analysis. *Hydrol.*
439 *Earth System Sci.* 13, 913–921.
- 440 Ding, Y., & Wang, S. S. Y. (2012). Optimal Control of Flood Diversion in Watershed Using Nonlinear 1 Optimization
441 2 3. *Advances in Water Resources*, 44, 30–48.
- 442 Domeneghetti, A., Molari, G., Tourian, M.T., Tarpanelli, A., Behnia, S., Moramarco, T., Sneeuw, T., Brath, A.,
443 (2021). Testing the use of single- and multi-mission satellite altimetry for the calibration of hydraulic
444 models. *Advances in Water Resources*, Volume 151, <https://doi.org/10.1016/j.advwatres.2021.103887>.



- 445 Domeneghetti, A., Tarpanelli, A., Brocca, L., Barbetta, S., Moramarco, T., Castellarin, A., & Brath, A. (2014). The use
446 of remote sensing-derived water surface data for hydraulic model calibration. *Remote Sensing of*
447 *Environment*, 149, 130–141. <https://doi.org/10.1016/J.RSE.2014.04.007>
- 448 Dubey, A. K., Gupta, P. K., Dutta, S., & Singh, R. P. (2015). An improved methodology to estimate river stage and
449 discharge using Jason-2 satellite data. *Journal of Hydrology*, 529, 1776–1787.
450 <https://doi.org/10.1016/j.jhydrol.2015.08.009>
- 451 Durand, M., Fu, L. L., Lettenmaier, D. P., Alsdorf, D. E., Rodriguez, E., & Esteban-Fernandez, D. (2010). The surface
452 water and ocean topography mission: Observing terrestrial surface water and oceanic submesoscale eddies.
453 *Proceedings of the IEEE*, 98(5), 766–779. <https://doi.org/10.1109/JPROC.2010.2043031>
- 454 Durand, M., Gleason, C. J., Garambois, P. A., Bjerklie, D., Smith, L. C., Roux, H., Rodriguez, E., Bates, P. D., Pavelsky,
455 T. M., Monnier, J., Chen, X., di Baldassarre, G., Fiset, J. M., Flipo, N., Frasson, R. P. D. M., Fulton, J., Goutal, N.,
456 Hossain, F., Humphries, E., ... Vilmin, L. (2016). An intercomparison of remote sensing river discharge
457 estimation algorithms from measurements of river height, width, and slope. *Water Resources Research*,
458 52(6), 4527–4549. <https://doi.org/10.1002/2015WR018434>
- 459 Fischer, C., Montmerle, T., Berre, L., Auger, L., & Ștefănescu, S. E. (2005). An overview of the variational
460 assimilation in the ALADIN/France numerical weather-prediction system. *Quarterly Journal of the Royal*
461 *Meteorological Society*, 131(613), 3477–3492. <https://doi.org/10.1256/QJ.05.115>
- 462 Frappart, F., Calmant, S., Cauhopé, M., Seyler, F., & Cazenave, A. (2006). Preliminary results of ENVISAT RA-2-
463 derived water levels validation over the Amazon basin. *Remote Sensing of Environment*, 100(2), 252–264.
464 <https://doi.org/10.1016/J.RSE.2005.10.027>
- 465 Frasson, R. P. de M., Durand, M. T., Larnier, K., Gleason, C., Andreadis, K. M., Hagemann, M., Dudley, R., Bjerklie, D.,
466 Oubanas, H., Garambois, P. A., Malaterre, P. O., Lin, P., Pavelsky, T. M., Monnier, J., Brinkerhoff, C. B., & David,
467 C. H. (2021). Exploring the Factors Controlling the Error Characteristics of the Surface Water and Ocean
468 Topography Mission Discharge Estimates. *Water Resources Research*, 57(6), e2020WR028519.
469 <https://doi.org/10.1029/2020WR028519>
- 470 Fu, L.-L., Alsdorf, D., Rodriguez, E., Morrow, R., Mognard, N., Lambin, J., Vaze, P., & Lafon, T. (2009). *The SWOT*
471 *(Surface Water and Ocean Topography) Mission: Spaceborne Radar Interferometry for Oceanographic and*
472 *Hydrological Applications*.
- 473 Garkoti, A., & Kundapura, S. (2021). Deriving water level and discharge estimation using satellite altimetry for
474 Krishna River, Karnataka. *Remote Sensing Applications: Society and Environment*, Volume 22.
475 <https://doi.org/10.1016/j.rsase.2021.100487>.
- 476 Gauthier, P., Tanguay, M., Laroche, S., Pellerin, S., & Morneau, J. (2007). Extension of 3DVAR to 4DVAR:
477 Implementation of 4DVAR at the Meteorological Service of Canada. *Monthly Weather Review*, 135(6), 2339–
478 2354. <https://doi.org/10.1175/MWR3394.1>
- 479 Getirana, A. C. V., & Peters-Lidard, C. (2013). Estimating water discharge from large radar altimetry datasets.
480 *Hydrology and Earth System Sciences*, 17(3), 923–933. <https://doi.org/10.5194/HESS-17-923-2013>.
- 481 Ghimire, E., Sharma S., & Lamichhane, N., (2022) Evaluation of one-dimensional and two-dimensional HEC-RAS
482 models to predict flood travel time and inundation area for flood warning system, *ISH Journal of Hydraulic*
483 *Engineering*, 28:1, 110-126, DOI: 10.1080/09715010.2020.1824621
- 484 Herschy, R., 1993. The stage–discharge relation. *Flow Meas. Instrum.* 4, 11–15.
- 485 Horritt, M.S., Bates, P.D., 2002. Evaluation of 1D and 2D numerical models for predicting river flood inundation.
486 *Journal of Hydrology*, 268, 87–99.
- 487 Jena, P.P., Chatterjee, C., Pradhan, G., Mishra, A. (2014). Are recent frequent high floods in Mahanadi basin in
488 eastern India due to increase in extreme rainfalls?, *Journal of Hydrology*, 517, 847–862.



- 489 Kebede, M.G., Wang, L., Li, X., & Hu, Z. (2020) Remote sensing-based river discharge estimation for a small river
490 flowing over the high mountain regions of the Tibetan Plateau, *International Journal of Remote Sensing*,
491 41:9, 3322-3345, DOI: 10.1080/01431161.2019.1701213
- 492 Lang, M., Pobanz, K., Renard, B., Renouf, E., Sauquet, E., 2010. Extrapolation of rating curves by hydraulic
493 modelling, with application to flood frequency analysis. *Hydrol. Sci. J.* 55 (6), 883–898.
494 <https://doi.org/10.1080/02626667.2010.504186>.
- 495 Leon, J. G., Calmant, S., Seyler, F., Bonnet, M. P., Cauhopé, M., Frappart, F., Filizola, N., & Fraizy, P. (2006). Rating
496 curves and estimation of average water depth at the upper Negro River based on satellite altimeter data
497 and modeled discharges. *Journal of Hydrology*, 328(3–4), 481–496.
498 <https://doi.org/10.1016/j.jhydrol.2005.12.006>
- 499 Mansanarez, V., Westerberg, I.K., Lam, N., Lyon, S.W., (2019). Rapid Stage-Discharge Rating Curve Assessment
500 Using Hydraulic Modeling in an Uncertainty Framework. *Water Resour. Res.* 55, 9765–9787.
- 501 Michailovsky, C. I., Milzow, C., & Bauer-Gottwein, P. (2013). Assimilation of radar altimetry to a routing model of
502 the Brahmaputra River. *Water Resources Research*, 49(8), 4807–4816.
503 <https://doi.org/10.1002/WRCR.20345>
- 504 Milzow, C., Krogh, P. E., & Bauer-Gottwein, P. (2011). Combining satellite radar altimetry, SAR surface soil
505 moisture and GRACE total storage changes for hydrological model calibration in a large poorly gauged
506 catchment. *Hydrology and Earth System Sciences*, 15(6), 1729–1743. [https://doi.org/10.5194/HESS-15-
507 1729-2011](https://doi.org/10.5194/HESS-15-1729-2011)
- 508 N.R.S.C., (2006). National Land Use and Land Cover Mapping using AWiFS. Data, Project Report. Hyderabad, India.
- 509 Oki, T., & Kanae, S. (2006). Global hydrological cycles and world water resources. *Science*, 313(5790), 1068–1072.
510 [https://doi.org/10.1126/SCIENCE.1128845/ASSET/FD158228-41CA-4074-9C78-
511 0C52F16C1FF3/ASSETS/GRAPHIC/313_1068_F3.JPEG](https://doi.org/10.1126/SCIENCE.1128845/ASSET/FD158228-41CA-4074-9C78-0C52F16C1FF3/ASSETS/GRAPHIC/313_1068_F3.JPEG)
- 512 Oubanas, H., Gejadze, I., Malaterre, P. O., Durand, M., Wei, R., Frasson, R. P. M., & Domeneghetti, A. (2018).
513 Discharge Estimation in Ungauged Basins Through Variational Data Assimilation: The Potential of the SWOT
514 Mission. *Water Resources Research*, 54(3), 2405–2423. <https://doi.org/10.1002/2017WR021735>
- 515 Oubanas, H., Gejadze, I., Malaterre, P. O., & Mercier, F. (2018). River discharge estimation from synthetic SWOT-
516 type observations using variational data assimilation and the full Saint-Venant hydraulic model. *Journal of*
517 *Hydrology*, 559, 638–647. <https://doi.org/10.1016/j.jhydrol.2018.02.004>
- 518 Paiva, R. C. D., Collischonn, W., Bonnet, M. P., de Gonçalves, L. G. G., Calmant, S., Getirana, A., & Santos Da Silva, J.
519 (2013). Assimilating in situ and radar altimetry data into a large-scale hydrologic-hydrodynamic model for
520 streamflow forecast in the Amazon. *Hydrology and Earth System Sciences*, 17(7), 2929–2946.
521 <https://doi.org/10.5194/HESS-17-2929-2013>
- 522 Papa, F., Bala, S. K., Pandey, R. K., Durand, F., Gopalakrishna, V. v., Rahman, A., & Rossow, W. B. (2012). Ganga-
523 Brahmaputra river discharge from Jason-2 radar altimetry: An update to the long-term satellite-derived
524 estimates of continental freshwater forcing flux into the Bay of Bengal. *Journal of Geophysical Research:*
525 *Oceans*, 117(11). <https://doi.org/10.1029/2012JC008158>
- 526 Parhi, P.K., Mishra, S.K., Singh, R., Tripathy, V.K., 2012. Floods in Mahanadi river basin, Orissa (India): a critical
527 review. *India Water Week, Water, Energy and Food Security: Call for Solutions*, 10–14 April 2012, New
528 Delhi.
- 529 Parhi, P. (2013). "HEC-RAS model for Manning's roughness: A case study." *Open J. Mod. Hydrol.*, 03, 97–101.
530 doi:<https://doi.org/10.4236/ojmh.2013.33013>.
- 531 Paris, A., Dias de Paiva, R., Santos da Silva, J., Medeiros Moreira, D., Calmant, S., Garambois, P. A., Collischonn, W.,
532 Bonnet, M. P., & Seyler, F. (2016). Stage-discharge rating curves based on satellite altimetry and modeled



- 533 discharge in the Amazon basin. *Water Resources Research*, 52(5), 3787–3814.
534 <https://doi.org/10.1002/2014WR016618>
- 535 Pereira-Cardenal, S. J., Riegels, N. D., Berry, P. A. M., Smith, R. G., Yakovlev, A., Siegfried, T. U., & Bauer-Gottwein, P.
536 (2011). Real-time remote sensing driven river basin modeling using radar altimetry. *Hydrology and Earth*
537 *System Sciences*, 15(1), 241–254. <https://doi.org/10.5194/HESS-15-241-2011>
- 538 Rabier, F., Järvinen, H., Klinker, E., Mahfouf, J. F., & Simmons, A. (2007). The ECMWF operational implementation
539 of four-dimensional variational assimilation. I: Experimental results with simplified physics. *Quarterly*
540 *Journal of the Royal Meteorological Society*, 126(564), 1143–1170.
541 <https://doi.org/10.1002/QJ.49712656415>
- 542 Rai, A. K., Beg, Z., Singh, A., & Gaurav, K. (2021). Estimating discharge of the Ganga River from satellite altimeter
543 data. *Journal of Hydrology*, 603. <https://doi.org/10.1016/j.jhydrol.2021.126860>
- 544 Samantaray, S., & Sahoo, A., (2020). Estimation of flood frequency using statistical method: Mahanadi River basin,
545 India. *H2Open Journal*, 3 (1), 189–207. doi: <https://doi.org/10.2166/h2oj.2020.004>
- 546 Shustikova, I., Domeneghetti, A., Neal, J.C., Bates P., & Castellarin, A. (2019) Comparing 2D capabilities of HEC-
547 RAS and LISFLOOD-FP on complex topography, *Hydrological Sciences Journal*, 64:14, 1769-
548 1782, DOI: [10.1080/02626667.2019.1671982](https://doi.org/10.1080/02626667.2019.1671982)
- 549 Tarpanelli, A., Barbetta, S., Brocca, L., & Moramarco, T. (2013). River Discharge Estimation by Using Altimetry
550 Data and Simplified Flood Routing Modeling. *Remote Sensing 2013, Vol. 5, Pages 4145-4162*, 5(9), 4145–
551 4162. <https://doi.org/10.3390/RS5094145>
- 552 Thakur, P. K., Garg, V., Kalura, P., Agrawal, B., Sharma, V., Mohapatra, M., Kalia, M., Aggarwal, S. P., Calmant, S.,
553 Ghosh, S., Dhote, P. R., Sharma, R., & Chauhan, P. (2021). Water level status of Indian reservoirs: A synoptic
554 view from altimeter observations. *Advances in Space Research*, 68(2), 619–640.
555 <https://doi.org/10.1016/j.asr.2020.06.015>
- 556 Tourian, M. J., Schwatke, C., & Sneeuw, N. (2017). River discharge estimation at daily resolution from satellite
557 altimetry over an entire river basin. *Journal of Hydrology*, 546, 230–247.
558 <https://doi.org/10.1016/j.jhydrol.2017.01.009>
- 559 Wahr, J. M., 1985. Deformation induced by polar motion. *Journal of Geophysical Research: Solid Earth* (1978–
560 2012), 90(B11), 9363–9368.
- 561 Wilson, M. D., Bates, P., Alsdorf, D., Forsberg, B., Horritt, M., Melack, J., Frappart, F., & Famiglietti, J. (2007).
562 Modeling large-scale inundation of Amazonian seasonally flooded wetlands. *Geophysical Research Letters*,
563 34(15), 15404. <https://doi.org/10.1029/2007GL030156>
- 564 Zakharova, E., Nielsen, K., Kamenev, G., & Kouraev, A. (2020). River discharge estimation from radar altimetry:
565 Assessment of satellite performance, river scales and methods. *Journal of Hydrology*, 583.
566 <https://doi.org/10.1016/j.jhydrol.2020.124561>

567